International Journal of GEOMATE, March., 2018 Vol.14, Issue 43, pp.112-117
Geotec., Const. Mat. & Env., DOI: https://doi.org/10.21660/2018.43.3578
ISSN: 2186-2982 (Print), 2186-2990 (Online), Japan

PLASTIC FLOW HETEROGENEITY AND FAILURE OF BIMETAL MATERIAL

Svetlana Barannikova, Lev Zuev and *Yulia Li

Institute of Strength Physics and Materials Science, SB RAS, 2/4 Academicheskii Ave., Tomsk, Russia

*Corresponding Author, Received: 14 July 2017, Revised: 19 Dec. 2017, Accepted: 15 Jan. 2018

ABSTRACT: The aim of this paper was to display the kinetics of Lüders band (LB) propagation of bimetallic material on the yield plateau at the microscale level. The localization patterns of plastic deformation in the process of uniaxial tension were obtained by the non-contact method of recording the fields of displacement vectors. The microstructure of the interfaces with the user results of optical, atomic force and scanning microscopy showed that in the direction of the pearlite steel to the austenitic form there are structural components: the weakened zone of the ferrite layer; a hardened section of the ferrite layer dark-pickling layer from the side of the austenitic steel. Plastic deformation of a bimetal began from the nucleation of the Lüders band on the boundaries of the bimetal on stress raisers with higher hardness due to the diffusion effect. In the main layer, the Lüders band was limited to a pair of fronts moving in opposite directions along the bimetal axis with different velocities. The cladding layer did not suppress the formation of Lüders bands, led to an increase in the propagation velocity of Lüders band fronts in the base layer.

Keywords: Lüders band, Localization of plastic deformation, DIC, steel, bimetal

1. INTRODUCTION

The development of instability and associated localization of plastic deformation of metals and alloys always follow the plastic flow phenomenon. The emergence of instability refers to the phenomenon arising in the transition from the uniform deformation to the state when deformations are localized at comparatively small areas.

Unstable plastic deformation of metals and alloys at the macroscopic level is manifested in the form of a sharp yield point, neck formation and discontinuous deformation [1-3]. The bands of micro localized deformation accompanying jumps of deformation and/or stresses impair the industrial products surface quality, cause their premature corrosion and increase the probability of sudden destruction. Studies of the nonuniformity of materials deformation had been previously made in detail on specimens of pure metals and alloys [4-6]. This paper considers the deformation behavior of a corrosion-resistant bimetal – carbon steel - stainless steel – which is used in chemical engineering for the manufacturing of reaction columns, autoclaves, reactors and heat exchangers [7-10]. The main requirement for a bimetal is to ensure the strength and ductility of the compound, its continuity, and stability of its properties over the entire contact surface. In this connection, it is necessary to improve knowledge about the processes of joining dissimilar metals and their joint plastic deformation on micro-, meso- and macroscale levels.

2. RESEARCH MATERIALS AND METHODS

The studied samples of bimetallic compounds were cut from a strip produced according to the following procedure: between the sheets of cladding metal put into the mold box - 321 AISI as a parent metal steel of A 283 Grade C was poured ($t = 1500°C$), followed by hot rolling of the obtained three-layer sheet at $t = 1200 \div 1400°C$. Along the outer edge of the sample on both sides ≈ 750 microns thick cladding layer of 321 AISI steel is located; in the center ≈ 6.7 mm thick layer of the base metal of A 283 Grade C.

Sample preparation of the bimetal for metallographic studies and visualization of zones of large deformation localization was carried out according to the standard procedure for steels and alloys: grinding on abrasive cloths of various grades: 50H 865, M50 L219, P120; polishing using diamond paste ACM 1/0 on a felt base. Chemical etching of the sample was carried out with reagents to reveal structures of stainless and low-carbon steels.

Pre-prepared samples in the form of a double dog bone with the dimensions of the working section $42\times8\times2$ mm were extended at T = 300K at a rate of $6{,}67\times10^{-5}c^{-1}$ on an LFM-125 test machine.

Visualization of the localized plastic deformation bands and registration of their proliferation kinetics was carried out at the working portion of the sample by the length of 42 mm by two non-contact methods: the method of digital image speckle correlation and the method of digital statistic speckle photography [11,12]. When these methods were implemented, the extended sample was illuminated with coherent light of a semiconductor laser with a wavelength of 635nm and a power of 15W. The strained sample images obtained in this light and superimposed with speckle patterns were recorded with PixelLink PL-B781 digital video camera at the frequency of 10Hz and the resolution of 15.114 microns/pixel, digitized and stored as files. The idea of the method of digital correlation of speckle images is in the possibility to determine displacement fields with a high accuracy by tracking changes in the material surface and comparing the digital images recorded during stressing. In the method of digital statistical speckle photography, a count sequence for each picture point of a speckle image structure was formed characterizing the time course of its brightness, variance and the expectation were calculated and the ratio between them was used for mapping zones of plastic deformation localization.

3. RESULT AND DISCUSSION

The study of the microstructure by optical metallography has allowed establishing that after rolling of a three-layer sample, the interfaces of dissimilar materials are clear and thin, pores and nonmetallic inclusions are absent, which indicates continuity and high quality of the engagement.

Examination of the bimetal conjugation area using the LEO EVO 50 scanning electron microscope (Carl Zeiss, Germany) with the Oxford Instruments attachment for X-ray dispersion microanalysis (NANOTECH Center of the Institute of Theoretical and Experimental Physics affiliated with SB RAS) yielded data on the quantitative content of elemental composition of steels in the conjugation area in the course of a step-by-step approximation to the boundary, as, for instance, shown in Fig. 1.

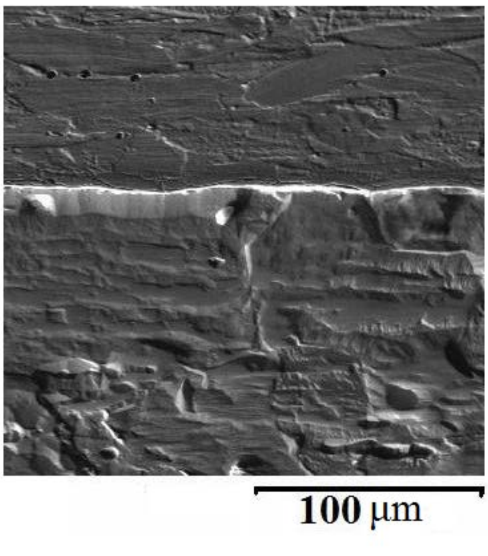

Fig. 1 Bimetal areas for dispersive microanalysis (5 μm distance to the conjugation boundary).

The results of the study of the quantitative elemental composition of steels in the conjugation area showed a chromium content in the steel of 321 AISI, the concentration of which increases from 0.18 to 0.39 (wt.%) in the direction of the conjugation boundary between 25 and 5 μm. At the same time, in the stainless steel, in the direction of the conjugation boundary between the two sheets of steel, the chromium content decreases, due to the diffusion of chromium from stainless steel in 321 AISI. Since carbon belongs to chemical elements with a low sequence number, in this case, only its qualitative assessment is possible. Analysis of the carbon content in stainless steel at the depth of 10 μm from the conjugation boundary between the two metals has shown an increase of 0.32 (wt.%). At the same distance and less than 10 μm from the conjugation boundary, carbides are formed as a result of diffusion of alloying elements from steel A 283 Grade C into 321 AISI, which explains the increased hardness of structural steel in the conjugation area.

The results of the investigation of the microhardness distribution along the thickness of the bimetallic compound are shown in Fig. 2. Thus, the microhardness at the conjugation was significantly higher than the microhardness of the base metal (321 AISI) and the cladding layer (A 283 Grade C) outside the conjugation area. Such a change in the microhardness along the width of the conjugation zone can be explained by the manifestation of two competing effects due to the presence of directed flows: carbon from low-carbon steel 321 AISI into stainless steel A 283 Grade C, and alloying elements Cr and Ni in the opposite direction. The first stream leads to softening and formation of a ferrite structure in the border sections of 321 AISI, which originally had a perlite structure, and the second, on the contrary, leading to their hardening.

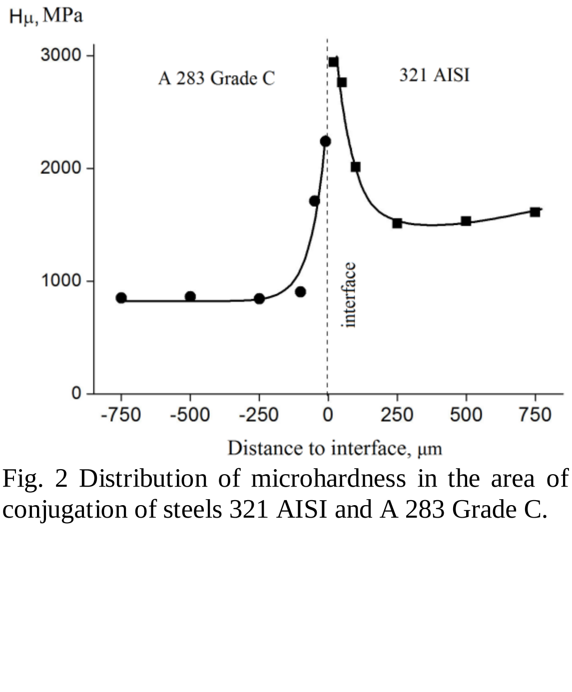

Fig. 2 Distribution of microhardness in the area of conjugation of steels 321 AISI and A 283 Grade C.

In steel 321 AISI the basis is ferrite, and in steel A 283 Grade C it is austenite (Fig. 3) [3].

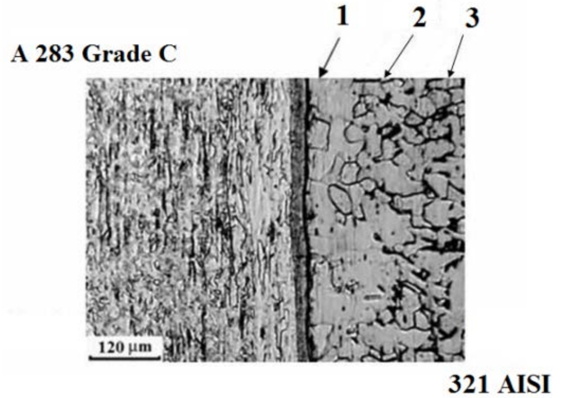

Fig. 3 Optical metallography of bimetal in the conjugation area: (1) – the decarburized layer – the conjugation area; (2) – the zone of partial decarburization; (3) – the structure of the base metal (321 AISI).

Fig. 4 (a-c) shows atomic force microscopy scan images taken when examining the structure of the base metal of 321 AISI, with a successive approximation to the boundary of conjugation with the cladding layer of stainless steel on an atomic force microscope. Thus in Fig. 4a the image of the structure of the base metal 321 AISI is obtained at the distance of ≈ 2 mm from the conjugation boundary and represents a matrix of ferrite with perlite colonies, which is a typical picture for low-carbon steels. A successive approximation to the conjugation boundary at a distance of about 200 μm makes it possible to detect an area of partial decarburization, which is transitional from the structure of the base metal to the ferrite structure (see Fig. 4b).

Further in Fig. 4c directly shows the conjugation boundary between the two metals. It is clearly seen that a decarburized layer consisting entirely of ferrite grains is formed on the side of the base metal of 321 AISI That means that a structure of pure ferrite was formed.

Let us consider in more detail the zone of partial decarburization of the structure of 321 AISI steel in the case of the AFM analysis. From the scan images (Fig. 5a) it follows that along the boundaries of the ferrite grains there are small spots of perlite, which is located between the grains of ferrite in the form of separate inclusions or interlayers. Studies have shown that the perlite cementite in 321 AISI is represented with thin, parallel plates, alternating with ferrite plates. Fig. 5b shows the fragmented structure of a pearlitic grain. It is shown that the cementite plates have an intermittent appearance, which may indicate a heterogeneous release of cementite within a single grain, and they can be unequal in thickness and curved.

It should be noted that the results are shown in Fig. 3-4 were obtained directly by observing the surface of a metallographic section made by means of traditional methods without the manufacture of special preparations (foils) required for electron microscopy by the method of AFM**.**

(a)

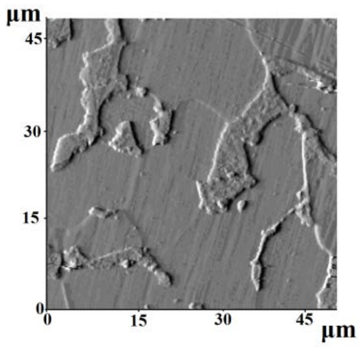

(b)

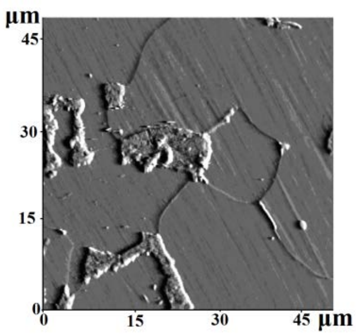

(c)

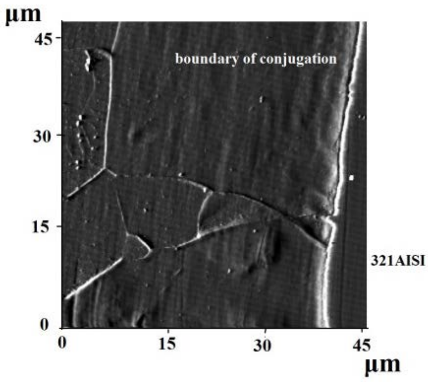

Fig. 4 An atomic-force image of the bimetal structure in the conjugation area: (a) the base metal structure; (b) the zone of partial decarburization; (c) the decarburized layer - the conjugation area.

Loading curves of flat samples of bimetal, and the samples equal in size made separately from steels 321 AISI and A 283 Grade C are presented in Figure 6. They cover the areas of elastic and large deformations and the area of the fracture. The bimetal curve after the yield point in the area of large deformations is located between the curves for its components (20 samples from each material were tested).

(a)

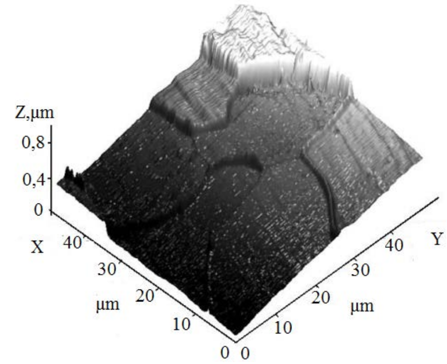

(b)

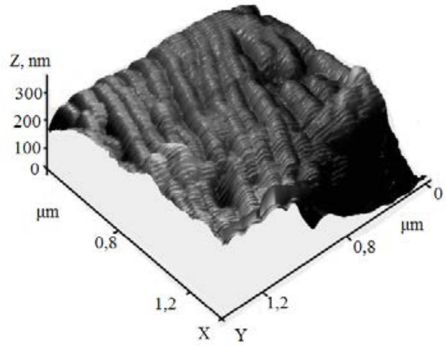

Fig. 5 An atomic-force image of the bimetal structure in the zone of partial decarburization;(a) a 3D image; (b) features of perlite structure.

On the loading curves for 321 AISI and the bimetal, the pronounced tooth and the yield plateau are visible, on which the oscillations of the deforming stress are noticeable (Fig. 6).

The presence of a cladding layer of stainless steel leads to a reduction in the duration of the yield plateau, an increase in the strength limit, and a decrease in the ductility of the base metal (321 AISI). For complete coverage of the processes of nucleation and development of Lüders bands (LB) in the bimetal, during the experiments, the registration of speckle images began at a voltage lower than the yield strength and ceased at the completion of the yield plateau and transition to the stage of strain hardening.

As the experiment showed, the large deformation in the bimetal sample is localized first in the form of an LB nuclei, which appears on the yield drop (point A in the inset of Figure 6), i.e., at the stage of micro large deformation. Fig. 7a shows that the Lüders band front (1) arises at the upper conjugation boundary of the cladding layer, the main layer of the bimetal, and germinates in the base layer of 321 AISI. Along with this (Fig. 7b), at the lower conjugation boundary of the cladding layer (the main layer of the bimetal), the second Lüders band front (2) is generated (point B in the inset of Figure 6).

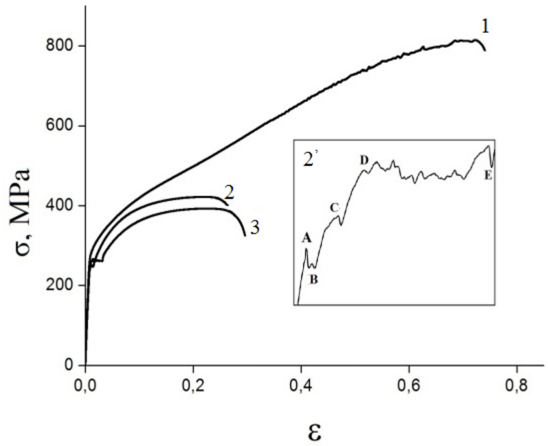

Fig. 6 Loading curves: 1 - A 283 Grade C; 2 - bimetal; 3 – 321 AISI; 2' is the yield surface of curve 2 for the bimetal.

At the bimetal flow plateau (inset of Fig. 6), the growth of the embryo of the strip across the sample corresponds to the formation of the ascending branches of the BC for the front of the Lüders band (1) and the CD for the Lüders bands (2).

(a)

(b)

(c)

Fig. 7 Origin of the Lüders band fronts of the bimetal at the plateau: (a) ε = 0.0081; (b) ε = 0.0084; (c) ε = 0,0099.

At the moment when both embryos cross the entire section of the bimetal, the formation of the Lüders band ends and its expansion begins. In the bimetal expansion diagram, this process corresponds to the DE area of the yield plateau. The generated Lüders band is limited by a pair of fronts moving in opposite directions along the axis of the sample at velocities ± V_f, and gradually transferring the bimetal from the elastic to the plastic state.

An important characteristic of the process is the speed of motion of the LB fronts. It was found out that when the LB starts, its two fronts move in the main layer of 321 AISI in opposite directions with different velocities $V_1 = 0.8 \cdot 10^{-4}$ m/s and $V_2 = 2.3 \cdot 10^{-4}$ m/s (Fig. 8a). Since the deformation is due to the more complex resistance of the bimetal to the loading compared to its components, the plastic flow at the initial stage is effected by means of propagation of the LB front in the basic soft metal, while the stronger cladding layer of stainless steel is deformed even more elastically.

(a)

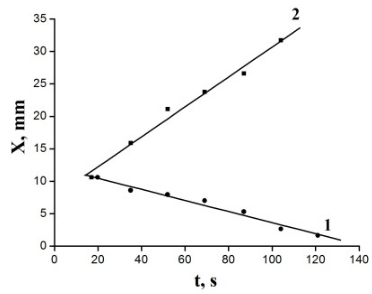

(b)

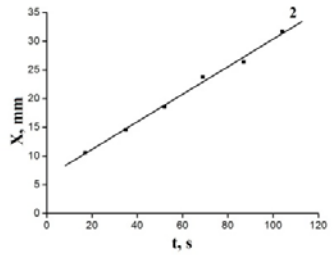

(c)

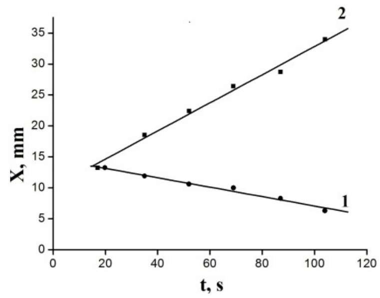

Fig. 8 Propagation of Lüders bands fronts in the bimetal at the yield plateau: (a) in the main layer of 321 AISI (ML), (b) in the upper cladding layer (CL), (c) in the lower cladding layer of A 283 Grade C.

Then, the base layer and the cladding layer of the bimetal are deformed plastically. As a result, in the upper cladding layer of the material A 283 Grade C only the Lüders band front (2) propagates with velocity $V_2 = 2.4 \cdot 10^{-4}$ m / s (Figure 8b), and two Lüders band fronts (1) and (2) propagate in the lower cladding layer (A 283 Grade C) in opposite directions with velocities $V_1 = 0.7 \cdot 10^{-4}$ m/s, $V_2 = 2.3 \cdot 10^{-4}$ m/s (Fig. 8c).

To compare the data, note that when analyzing the patterns of localization of large deformation of samples of 321 AISI low-carbon steel under tension, the following was revealed. The generation of LB fronts corresponds to the stress of the upper yielding tooth and occurs in the area of the base stress concentrator near the mobile gripper of the test machine (Fig. 9a). As a result, one LB front propagates throughout the yield plateau with the velocity $V_2 = 1.1 \cdot 10^{-4}$ m/s (Fig. 9b).

(a)

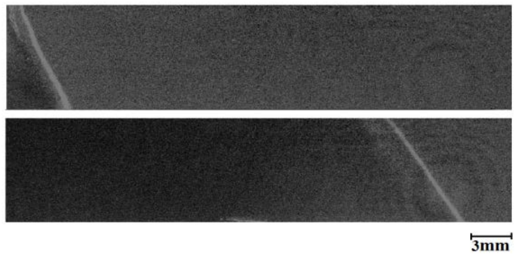

(b)

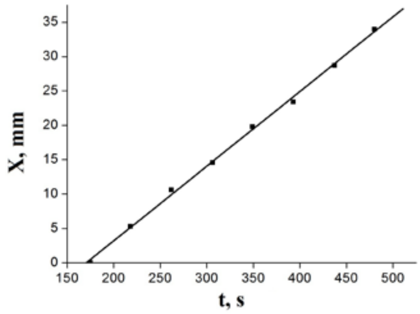

Fig. 9 Origin of the Lüders band front at the yield plateau of 321 AISI: (a) $\varepsilon = 0.008$ and $\varepsilon = 0.028$;(b) propagation of the CLB front at the yield plateau of 321 AISI.

The parabolic reveals plastic flow localization in the form of a stationary system of the plastic flow centers through the specimen length with the distance $\lambda = 4$ mm between them (Fig. 10).

At the pre-fracture stage, the immobile zones of plastic strain localization started moving consistently with a tendency to merge into a high-amplitude focus of localized straining, where a neck-like narrowing of the sample cross section was formed. This maximum forms at the place of occurring damage. The peculiarity of damage of the bimetal is related to the heterogeneity of plastic deformation in the intermediate layer of the metal.

Fragmentation of the specimen determines the fracture pattern of the bimetal composite. Two macro bands of localized plastic deformation are formed at the stage of the shoulder effect in the area of stress macro concentrator.

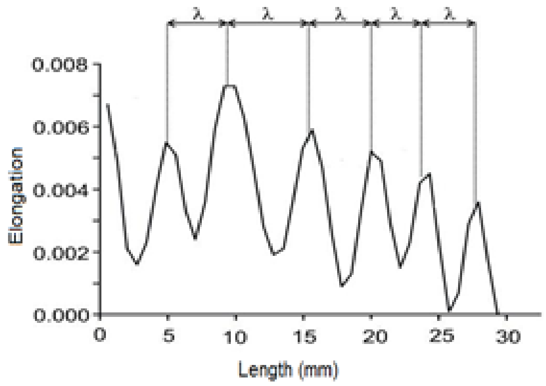

Fig. 10 The distribution of local elongation ε_{xx} along the axis of extension during of parabolic work hardening stage.

They propagate along conjugated directions of maximum shear stress across the whole section of the sample, forming trihedral prisms on the macro level on the bond interface of the bimetal. The cracks are nucleated in the area of parent metal at the trihedral prism tip, gradually merged passing across the whole section of the metal sample (Fig. 11).

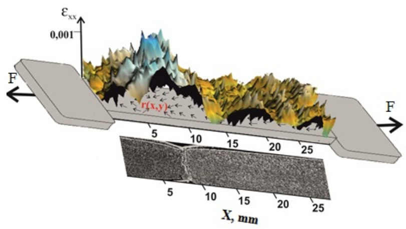

Fig. 11 Bimetal fracture patterns and distribution of local extensions at the prefracture stage under deformation 0.24.

4. CONCLUSION

The research conducted allowed to identify the main patterns of the proliferation of LB in the main layer material. It is revealed that the LB is limited to a pair of fronts moving in opposite directions along the bimetal axis with different propagation velocities. The cladding layer does not suppress the formation of LB, leading to an increase in the propagation speed of the LB fronts in the main layer. Metallographic studies have shown that at the extension of bimetallic samples of A 283 Grade C + 321 AISI a decarbonized layer is formed in bimetal at the side of A 283 Grade C steel, and at the side of 321 AISI steel, a carburized layer is formed. On the boundary of conjugation of bimetal layers, an intermediate layer (carbide) is found, by the depth of up to 50μm.

5. ACKNOWLEDGEMENTS

The work was supported by the Russian Science Foundation (project No. 16-19-10025).

6. REFERENCES

[1] Orlova D, Barannikova S, Zuev L, “On the kinetics of localized plasticity domains emergent at the pre-failure stage of deformation process”, AIP Conf. Proc. 2016, Vol.1783, pp. 020168.
[2] Danilov V.I, Barannikova S.A, Zuev L.B, “Localized strain autowaves at the initial stage of plastic flow in single crystals”, Tech. Phys. 2003, Vol. 48, pp. 1429-1435.
[3] Zuev L. B, Barannikova S. A, “Experimental study of plastic flow macro-scale localization process: Pattern, propagation rate, dispersion”, 2014, Int. J. Mec. Sci. Vol. 88, pp. 1-7.
[4] Acarer M, Gulenc B, Findik F, “Investigation of explosive welding parameters and their effects on microhardness and shear strength”, 2013, Mater.Des. Vol. 24, pp. 659-664.
[5] Venkateswara N, Madhusudhan G, Nagarjuna S, “Weld overlay cladding of high strength low alloy steel with austenitic stainless steel – Structure and properties”, 2011, S. Mater. Des. Vol. 32, pp. 2496-2506.
[6] Findik F, Yilmaz R, Somyurek T, “The effect of heat treatment on the microstructure and microhardness of explosive welding”, 2011, Acad. J. Vol. 6, pp. 4141-4151.
[7] Guobin L, Jianjun W, Xiangzhi L. Guiyun L, “The properties and application of bi-metal hot-forging die”, 1998, J. Mat. Proc. Tech. Vol. 75, pp. 152-156.
[8] Mehnen L, Pfutzner H, Kaniusas E, “Magnetostrictive amorphous bimetal sensors”, 2000, J. Magn.Magn. Mater. Vol. 215, pp. 779-781.
[9] Nakano J, Miwa Y, Tsukada T, Kikuchi M, Kita S, Nemoto Y, Tsuji H, Jitsukawa S, “Characterization of 316L(N)-IG SS joint produced by hot isostatic pressing technique”, 2002, J. Nucl. Mater. Vol. 307, pp. 1568-1572.
[10] Akramifarid H.R, Mirzadeh H, Parsa M.H, “Cladding of aluminum on AISI 304L stainless steel by cold roll bonding: Mechanism, microstructure, and mechanical properties”, 2014, Mater. Sci. Eng. Vol. A 613, pp. 232-239.
[11] Sozen S, “Determination of displacement distributions in welded steel tension elements using Digital image techniques”, Steel Comp. Str. Int. J., Vol. 18, pp. 1103-1117.
[12] Sokoli D, Shekarchi W, Buenrostro. E, Wassim M, “Advancing behavioral understanding and damage evaluation of concrete members using high-resolution digital image correlation data”, 2014, Earthquakes and Structures An Int'l Journal,Vol.7, pp.609-626.